Correcting Atmospheric Effects on the InSAR Measurements using GPS Data

Correcting Atmospheric Effects on the InSAR Measurements using GPS Data

Amir Sharifuddin Ab Latip[1], Andi Mohd Hairy Ansar[2*], Ami Hassan Md Din[2,3], Abdul Lateef Balogun[4]

[1] Centre of Studies for Surveying Science and Geomatics, Faculty of Architecture, Planning and Surveying, Universiti Teknologi MARA, 40450 Shah Alam, Selangor Darul Ehsan, Malaysia
[2] Geospatial Imaging and Information Research Group (GI2RG), [3]Geoscience and Digital Earth Centre (INSTeG), Faculty of Built Environment and Surveying, Universiti Teknologi Malaysia, 81310 Johor Bahru, Johor Darul Takzim, Malaysia
[4] Geospatial Analysis and Modelling Research Group (GAMR), Department of Civil and Environmental Engineering, Universiti Teknologi PETRONAS (UTP), 32610 Seri Iskander, Perak Darul Ridzuan, Malaysia

*Email: andimohdhairy@gmail.com

Abstract. The effect of the atmospheric error in the spaceborne synthetic aperture radar (SAR) signal is more prominent in Malaysia due to its hot and wet conditions. Because the atmospheric error is believed to happen constantly in space and randomly in time, low-pass filtering in space and high-pass filtering in time is employed to measure it. However, with few scenes, the filtering technique's reliability in removing atmospheric error may be insufficient, leading to erroneous surface deformation. Therefore, an external atmospheric correction needs to be modelled to improve the accuracy of surface deformation. In this study, the atmospheric error correction was estimated from GPS and applied to the deformation analysis. The result shows that the atmospheric error level estimated from the filtering technique was –6.9 to 7.5 radians, while using GPS was -1.0 to 1.9 radians. After using the filtering process, the rate of deformation fell dramatically. However, compared to the reference deformation, the rate was too low, indicating that the filtering technique overstated the level of atmospheric error. At many data collections, the atmospheric correction calculated from GPS gave deformation values closer to the reference deformation. Hence, this study will help the researchers to model the atmospheric correction over the Malaysia region in future.

1. Introduction

Microwave signals from Earth-orbiting satellites are used in the synthetic interferometric aperture radar (InSAR) technique to examine the deformation of the Earth's surface or man-made structures over time. [1], [2]. Surface area displacements may be easily identified and observed using InSAR methods [3]. However, there are several possible sources of inaccuracies that might degrade the precision of InSAR

measurements. The key constraints are satellite orbital errors, temporal and spatial decorrelation effects and atmospheric inaccuracies [4], [5]. These limitations are included in interferograms created from InSAR data, in addition to deformations. To extract the deformations as precisely as feasible, InSAR's processing requires the removal of such signals. Most of those signals can be modelled precisely enough except for atmospheric delays.

The atmospheric error affects the signal path and the signal's propagation velocity since the radar signal passes through the Earth's atmosphere twice. Changes in atmospheric variables, such as water vapour, pressure, and temperature, cause the signals to be delayed and the interferograms to be perturbed, hiding the deformations in some instances [6]. Atmospheric influences are a significant cause of mistakes in interferometric product interpretation in regards to topography and displacement. Several investigations have indicated that the water vapour distribution in the subtropics is responsible for the majority of the atmospheric signal in interferometric products [7]. One of the InSAR community's concerns is filtering tropospheric delays, where spatial and temporal oscillations predominantly induce tropospheric signal imperfection in InSAR data.

Several strategies exist to predict atmospheric delays based on various data or weather models [8]. A widely used phase-based technique (linear and power-law) outclasses the weather model in places where the atmospheric delay is mainly connected with topography. Another method used is using information from regional or worldwide weather models like pressure, temperature, and relative humidity. The Weather Research and Forecasting (WRF) model calculates hydrostatic and wet tropospheric delay [9]. However, none of these strategies precisely duplicate the uncertainties and provide high temporal resolution of results.

Commonly, atmospheric correction is estimated using GPS. There are many advantages of using GPS to evaluate and measure atmospheric corrections. The GPS has improved spatial-temporal resolution, is a low-cost technology, has global coverage, can be used in all weather conditions (not affected by rain and clouds), and is highly accurate and precise [10]. Since so much of the GPS Continuously Operating Reference Stations (CORS) network infrastructure was already in place, GPS was found to be acceptable for this task: calculating the atmospheric correction or Zenith Path Delay (ZPD) values without auxiliary equipment [11].

In InSAR processing, the filtering methodology implies that atmospheric error happens continuously in space and randomly in time. Low-pass and high-pass filtering in space and time are used to calculate atmospheric inaccuracy from existing data [12]. When only a few SAR scenes are employed, the filtering technique's resiliency in reducing atmospheric error may be limited, and the outcome is usually unhelpful. If the magnitude of deformation over time exhibits comparable patterns or temporal trend behaviours as the atmospheric inaccuracy, it may be filtered out or leaked into atmospheric estimates [13]. As a result, atmospheric error estimates are often omitted, and their contributions can be viewed as noise in the deformation analysis [14], [15]. However, because of the significant fluctuation of water vapour in this area, the deformation signal might be strongly impacted by atmospheric error at low latitude regions [16].

To process the radar satellite image and analyze the deformation signal from each measured Persistent Scatterer (PS) location, the Stanford Method for Persistent Scatterers (StaMPS) is used. The StaMPS approach incorporates the atmospheric correction predicted by the Global Positioning System (GPS) to reduce atmospheric error in data measurement.

2. Data and Methods

2.1. Study Area and Datasets

The study area involved in this study is one of the private Liquefied Natural Gas (LNG) Terminal in Bintulu. The terminal is located in Tanjung Kidurong, about 20 kilometres north of Bintulu town. It has a total area of 2.76 km2, making it one of the world's biggest ports and the only LNG liquefication plant in Malaysia. The terminal exports a substantial amount of LNG to Japan, South Korea, and Taiwan,

which helps Malaysia's socio-economic progress. The red rectangle demarcates the LNG terminal's interest area that study will be carried out as shown in Figure 1. The LNG complex was selected as the study area because it is located nearby to the coastal area which high amount of water vapour could be observed. Thus, the influence of water vapour in the LNG gives the significant impact on the InSAR measurement and need to be accounted for achieving high accuracy of the deformation estimation.

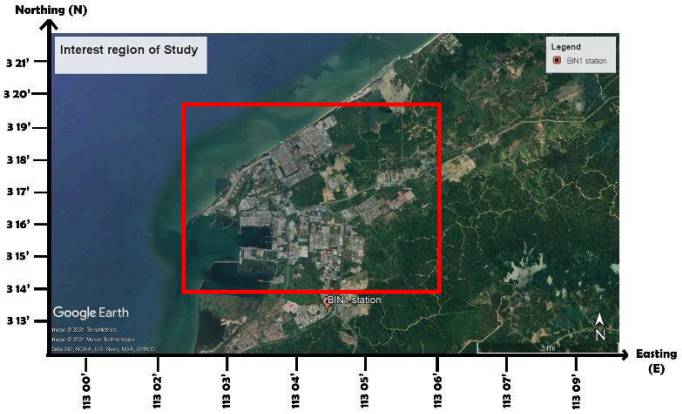

Figure 1. Interest region of the study

From April 21 to July 4, 2016, a SAR dataset of 10 TerraSAR-X images was taken over the LNG terminal, as shown in Table 1. The images were collected in a horizontal-horizontal (HH) polarisation mode along the ascending orbit (from South to North), with incidence angles varying from 49.57 to 51.11 degrees. StripMap imaging mode was employed with a sensor wavelength of 3.1 cm and a spatial resolution of 3 m in both azimuth and range directions. Each image covered a 30 km (width) by 50 km (length) area, covering the entire LNG complex. From all the available TerraSAR-X images, the image on October 14, 2015 (also indicated by the letter "M") was selected as a master image to reduce the effects of geometric and temporal decorrelation (other images referred to as slave images). It was chosen as the master image because it has the best temporal and spatial alignment of the slave images. The lowest and highest temporal and perpendicular baseline linkages were 44 days and 4 m and 264 days and 279 m.

Table 1. SAR datasets

Image number	Date (DD.MM.YYYY)	Perpendicular baseline (*Bberp*) [meters]	Temporal baseline (*Btemp*) [days]
1	21.04.2015	4	176
2	04.06.2015	-42	132
3	18.07.2015	82	88
4	31.08.2015	19	44
5	14.10.2015	0	0
6	27.11.2015	125	44
7	10.01.2016	279	88
8	23.02.2016	-53	132
9	25.05.2016	-105	220
10	04.07.2016	-22	264

The Malaysia Real-Time Kinematic GNSS network, known as MyRTKnet station, is used to acquire GPS data. The Malaysian Department of Surveying and Mapping (DSMM) established the MyRTKnet stations, a network of continually operational reference stations. In this investigation, 11 DSMM-operated MyRTKnet sites were combined with three additional IGS stations. There is only one nearest MyRTKnet station, BIN1 station. The other ten stations outside the scene were AMAN, BELA, LABI, LAWS, KAPI, MIRI, MRDI, MUKA, SIBI, and SARA. GPS data were collected at a sample rate of 30 seconds for 24 hours on the same day as the InSAR data. Because the GPS measurement may provide valid data in terms of horizontal and vertical deformations, the deformation rates obtained at the BIN1 MyRTKnet station can be utilised to assess the accuracy of the InSAR measurement.

2.2. Atmospheric correction from GPS data

The GPS satellites transmit microwave signals to GPS receivers on the ground, which travel through the Earth's atmosphere [17]. Signal propagation is slowed by dry gases (mostly nitrogen and oxygen) and water vapour in the troposphere (a layer up to 20 kilometres above the Earth's surface). Tropospheric delay is the term for this phenomenon [18], [19]. The entire tropospheric delay in the direction of each GPS satellite is known as the slant path delay (SPD). The SPD measurements are taken at various azimuth and elevation angles, resulting in varying amounts of tropospheric delay. Estimating each of the recorded SPDs and other parameters of interest (e.g., station locations) is impossible caused of a lack of redundancy data. Consequently, the SPD can be transferred to the vertical or zenith direction using a mapping function, resulting in the ZPD. To put it another way, the ZPD is the average of each of the measured SPD across time [16].

The Bernese GPS software 5.0 was used in post-processing mode to estimate ZPD for IGS and MyRTKnet stations [20], [21]. The ZPD was calculated using the programme after additional defects like satellite orbital errors, receiver location errors, ionospheric delays, and receiver and satellite clock difficulties were resolved or modelled. A low elevation angle of three degree was used during data processing to maximise the number of GPS observation data and improve the decorrelation between estimated station heights and ZPD [22]. The dry component, which was modelled using the a-priori Saastamoinen model, was mapped using the dry Niell mapping function. In contrast, the wet component was mapped using the wet Niell mapping function [23]. To avoid the non-realistic assumption of azimuthal symmetry utilised by both mapping functions, the gradient parameters were computed over 24 hours in north-south and east-west directions. The ZPD was calculated with a temporal precision of 1 hour over 24 hours and was calculated strictly at the SAR overpass time, which was then used to decrease atmospheric error in InSAR measurements.

The estimated ZPD from MyRTKnet stations was in millimetres, converted to radians (see Equation 1). In addition, as shown in Equation 2, the ZPD in the vertical direction was mapped to the radar SPD direction. The SPD values at the MyRTKnet stations were interpolated to the PS pixel locations using the Kriging interpolation method because the atmospheric signal is spatially linked. Kriging is a geostatistical interpolation method and can be implemented by the MATLAB language. This method depends on the distance and spatial relationship of the measured SPD values between MyRTKnet stations to predict the SPD values for the PS pixel locations. Figure 2 depicts the interpolation of SPD at GPS stations to PS locations and the projection of GPS ZPD into radar SPD. Figure 3 presents a flowchart of the method used for estimating atmospheric correction using GPS on InSAR measurement [24].

$$ZPD\_in\_rad=-4\pi/\lambda*(ZPD\_in\_mm) \quad (1)$$

$$Radar\_SPD=ZPD\_in\_rad/\cos(\theta) \quad (2)$$

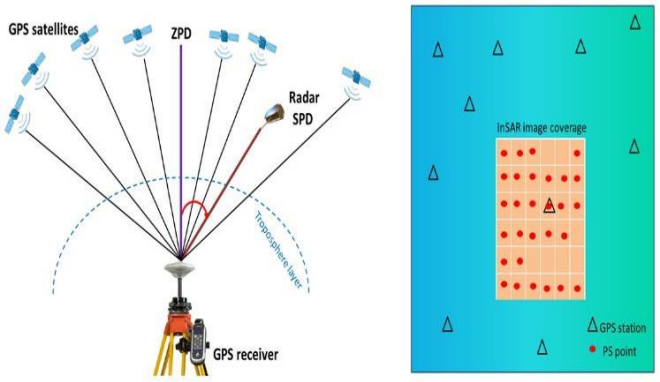

Figure 2. Projection of GPS ZPD to radar SPD and interpolation to PS points.

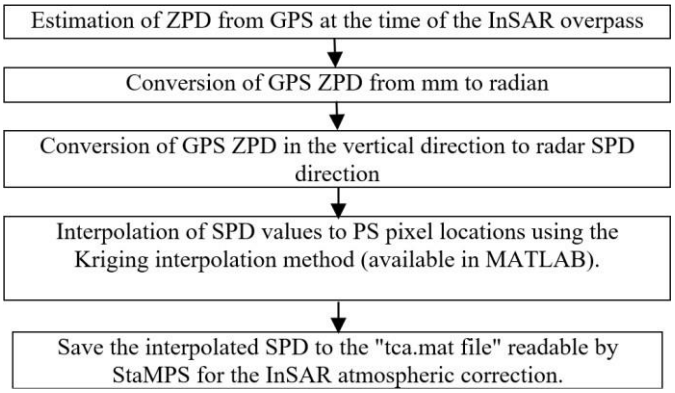

Figure 3. The proposed method for atmospheric error correction from GPS is depicted as a flowchart.

3. Result and Discussion

3.1. Applying Atmospheric Correction from GPS data

Figures 4 and 5 show the temporal and spatial measurements of the difference of the atmospheric errors concerning a selected reference image produced from GPS and filtering approaches, respectively. The atmospheric error level is determined by the length scale of water vapour changes in the atmosphere. The atmospheric error level decided using GPS data was between -1.0 and 1.9 radians, whereas the filtering technique was between –6.9 and 7.5 radians. The atmospheric delay levels predicted from GPS and the filtering approach differ significantly in this range of values. The estimated atmospheric inaccuracy from GPS fluctuated steadily across the whole image. As a result, because there is much variation in water vapour in low latitude regions and along the coast of the LNG terminal, the GPS is likely to underestimate the variations in water vapour in the atmosphere. Moreover, the accuracy of the interpolated atmospheric error at the PS pixel level is dependent on the spatial density of accessible GPS stations.

Figures 6 and 7 show the estimated ground deformation after accounting for atmospheric inaccuracy from GPS and the filtering process. After adding the GPS correction, the deformation rates range from -19.1 to 22.8 mm/yr, showing that the deformation rate was somewhat enhanced after the adjustment. As previously stated, GPS measurements cannot effectively reduce atmospheric error since the precision of interpolated water vapour is limited due to the sparse distribution of GPS stations. Nonetheless, the deformation rates ranged from -8.1 to 6.8 mm/yr after using the filtering method, demonstrating a considerable reduction in deformation rates.

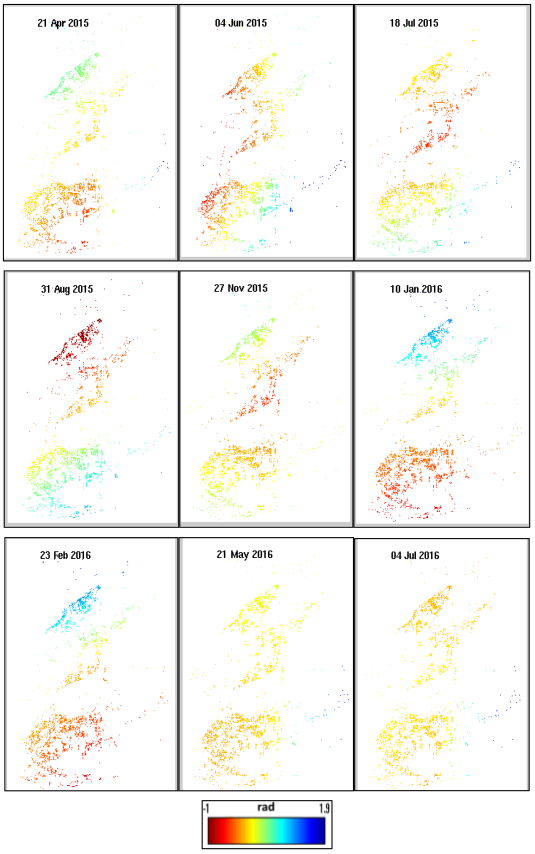

Figure 4. The spatial difference of atmospheric error estimated from the GPS.

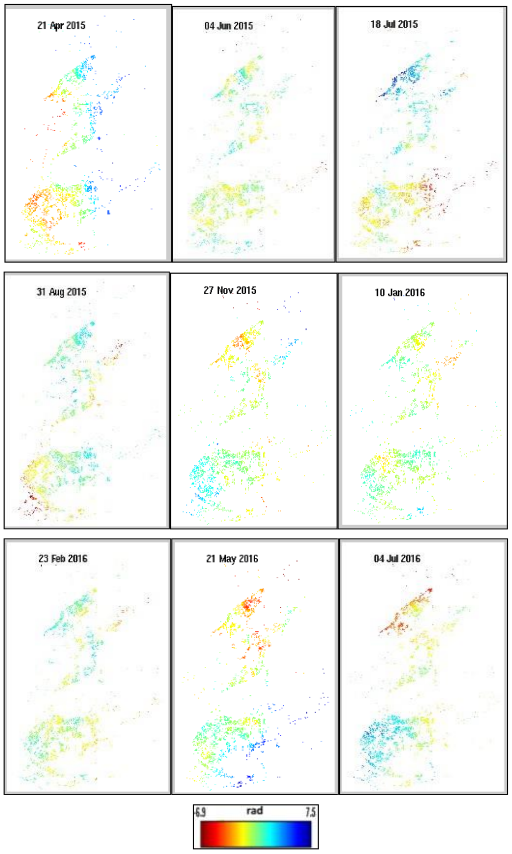

Figure 5. The spatial difference of atmospheric error estimated from filtering technique.

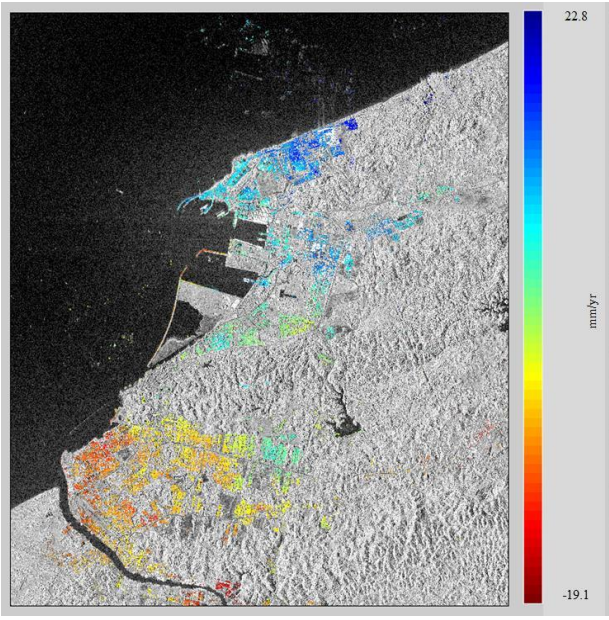

Figure 6. Upon correcting the atmospheric error with GPS data, the deformation estimation is performed.

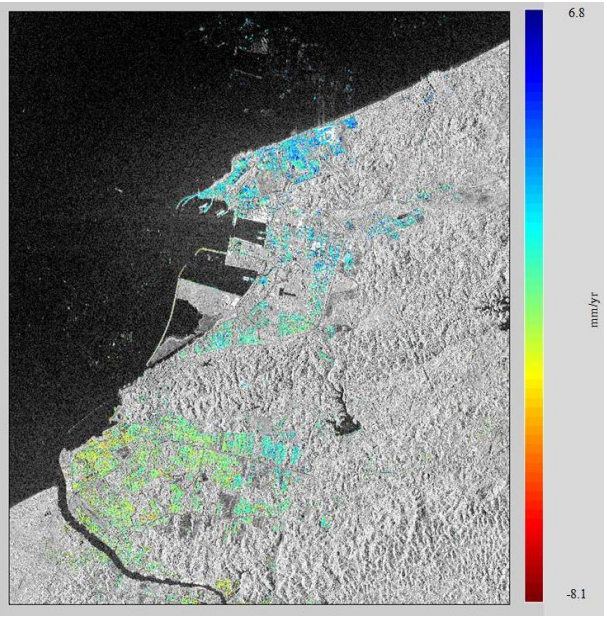

Figure 7. Upon correcting the atmospheric error with the filtering technique, the deformation estimation is performed.

3.2. Deformation Time-series Comparison

Figure 8 compares the deformation time series of the GPS as a reference, InSAR without atmospheric correction (InSAR v-d), InSAR with atmospheric correction from GPS (InSAR v-da), and InSAR with atmospheric correction from filtering approach (InSAR v-ds). At the second, third, seventh, ninth, and tenth data acquisitions, InSAR with atmospheric adjustment from GPS (InSAR v-da) gave ground deformation values that were closer to the reference ground deformation (GPS) than InSAR without atmospheric correction (InSAR v-d). InSAR with GPS atmospheric correction (InSAR v-da) lowered the InSAR-derived deformation rates by 40 to 86 percent compared to earlier data acquisitions, as seen in Table 2.

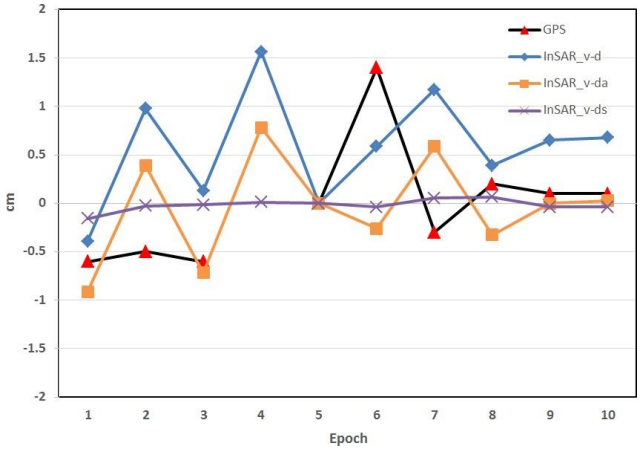

Figure 8. Deformation time series at the BIN1 MyRTKnet station are compared. The black line indicates the GPS-estimated deformation (reference). The other lines represented InSAR results from different techniques.

The deformation rate was significantly reduced after using the filtering technique (InSAR v-ds). However, it was too low compared to the reference deformation rate (GPS). As a result, the filtering algorithm overstated the amount of atmospheric error at the PS positions by accident. It indicates that if the deformation signal is large enough in space or drastically different from its temporal behaviour, it could be misconstrued as an atmospheric error.

Table 2. Performance of atmospheric correction from GPS data

Epoch	GPS (cm)	InSAR_v-d (cm)	InSAR_v-da (cm)	InSAR_v-ds (cm)	GPS - InSAR_v-d (cm)	GSPS - InSAR_v-da (cm)	Percentage of reduction
1	-0.6	-0.4	-0.9	-0.2	-0.2	0.3	
2	-0.5	1	0.4	0	-1.5	-0.9	40%
3	-0.6	0.1	-0.7	0	-0.7	0.1	86%
4	N/A	1.6	0.8	0	N/A	N/A	N/A
5	0	0	0	0	N/A	N/A	N/A
6	1.4	0.6	-0.3	0	0.8	1.7	
7	-0.3	1.2	0.6	0.1	-1.5	-0.9	40%
8	0.2	0.4	-0.3	0.1	-0.2	0.5	
9	0.1	0.7	0	0	-0.6	0.1	83%
10	0.1	0.7	0	0	-0.6	0.1	83%

4. Conclusion

At the second, third, seventh, ninth, and tenth data acquisitions, InSAR generated a ground deformation value closer to the reference ground deformation (GPS) after applying atmospheric correction from GPS compared to InSAR without atmospheric correction. The rate of distortion was significantly reduced after using the filtering method. However, the rate was meager compared to the reference deformation (GPS), showing that the filtering process exaggerated atmospheric error at the PS locations. Integration of GPS with MODerate Resolution Imaging Spectroradiometer (MODIS) data is recommended to enhance the precision of the atmospheric correction result. Because of the sparseness of GPS stations, MODIS has a higher spatial resolution of atmospheric water vapour than GPS, which has a 1 km spatial resolution.

Acknowledgements

We are grateful to the Universiti Teknologi Petronas for funding this research under the Yayasan Universiti Teknologi Petronas (YUTP-FRG) (0153AA-H15). Preparation of this paper is also partly supported by the Fundamental Research Grant Scheme, Ministry of Higher Education Malaysia (FRGS/1/2021/WAB07/UITM/02/1). Special thanks to the DSMM for providing the GNSS data in this study. Many thanks to Dr Abd Nasir Matori, who also took part in this research.

References

[1] Yu, C., Li, Z., & Penna, N. T. (2018). Interferometric synthetic aperture radar atmospheric correction using a GPS-based iterative tropospheric decomposition model. *Remote Sensing of Environment*, 204, 109–121. https://doi.org/10.1016/j.rse.2017.10.038

[2] Pepe, A., & Calò, F. (2017). A Review of Interferometric Synthetic Aperture RADAR (InSAR) Multi-Track Approaches for the Retrieval of Earth's Surface Displacements. *Applied Sciences*, 7(12), 1264. https://doi.org/10.3390/app7121264

[3] Shi, X., Xu, Q., Zhang, L., Zhao, K., Dong, J., Jiang, H., & Liao, M. (2019). Surface displacements of the Heifangtai terrace in Northwest China measured by X and C-band InSAR observations. *Engineering Geology*, 259, 105181. https://doi.org/10.1016/j.enggeo.2019.105181

[4] Tian, X., Malhotra, R., Xu, B., Qi, H., & Ma, Y. (2018). Modeling Orbital Error in InSAR Interferogram Using Frequency and Spatial Domain Based Methods. *Remote Sensing*, 10(4), 508. https://doi.org/10.3390/rs10040508

[5] Din, A. H. M., Zulkifli, N. A., Hamden, M. H., & Aris, W. A. W. (2019). Sea level trend over Malaysian seas from multi-mission satellite altimetry and vertical land motion corrected tidal data. *Advances in Space Research*, 63(11), 3452–3472. https://doi.org/10.1016/j.asr.2019.02.022

[6] Latip, A. S. A., Balogun, A. L., Din, A. H. M., & Ansar, A. M. H. (2021). The Use of InSAR for Monitoring Deformation of Offshore Platforms. *IOP Conference Series: Earth and Environmental Science*, 767(1), 012033. https://doi.org/10.1088/1755-1315/767/1/012033

[7] Kinoshita, Y., Morishita, Y., & Hirabayashi, Y. (2017). Detections and simulations of tropospheric water vapor fluctuations due to trapped lee waves by ALOS-2/PALSAR-2 ScanSAR interferometry. *Earth, Planets and Space*, 69(1). https://doi.org/10.1186/s40623-017-0690-7

[8] Liu, Y., Zhao, Q., Yao, W., Ma, X., Yao, Y., & Liu, L. (2019). Short-term rainfall forecast model based on the improved BP–NN algorithm. *Scientific Reports*, 9(1). https://doi.org/10.1038/s41598-019-56452-5

[9] Yáñez-Morroni, G., Gironás, J., Caneo, M., Delgado, R., & Garreaud, R. (2018). Using the Weather Research and Forecasting (WRF) Model for Precipitation Forecasting in an Andean Region with Complex Topography. *Atmosphere*, 9(8), 304. https://doi.org/10.3390/atmos9080304

[10] Sapucci, L. F., Machado, L. A. T., de Souza, E. M., & Campos, T. B. (2018). Global Positioning System precipitable water vapour (GPS-PWV) jumps before intense rain events: A potential application to nowcasting. *Meteorological Applications*, 26(1), 49–63. https://doi.org/10.1002/met.1735

[11] Vaquero-Martínez, J., & Antón, M. (2021). Review on the Role of GNSS Meteorology in Monitoring Water Vapor for Atmospheric Physics. *Remote Sensing*, 13(12), 2287. https://doi.org/10.3390/rs13122287
[12] Kirui, P. K., Reinosch, E., Isya, N., Riedel, B., & Gerke, M. (2021). Mitigation of Atmospheric Artefacts in Multi Temporal InSAR: A Review. *PFG – Journal of Photogrammetry, Remote Sensing and Geoinformation Science*. Published. https://doi.org/10.1007/s41064-021-00138-z
[13] Yu, C., Li, Z., & Penna, N. T. (2020). Triggered afterslip on the southern Hikurangi subduction interface following the 2016 Kaikōura earthquake from InSAR time series with atmospheric corrections. *Remote Sensing of Environment*, 251, 112097. https://doi.org/10.1016/j.rse.2020.112097
[14] Havazli, E., & Wdowinski, S. (2021). Detection Threshold Estimates for InSAR Time Series: A Simulation of Tropospheric Delay Approach. *Sensors*, 21(4), 1124. https://doi.org/10.3390/s21041124
[15] Karamvasis, K., & Karathanassi, V. (2020). Performance Analysis of Open Source Time Series InSAR Methods for Deformation Monitoring over a Broader Mining Region. *Remote Sensing*, 12(9), 1380. https://doi.org/10.3390/rs12091380
[16] Latip, A. S. A. (2012). Potentials of Global Positioning System for Meteorology in Low-latitude Region (Master's dissertation). Faculty of Goinformation and Real Estate, Universiti Teknologi Malaysia, Johor.
[17] Din, A. H. M., Reba, M. N. M., Omar, K. M., Ses, S., & Latip, A. S. A. (Eds.). (2015). Monitoring vertical land motion in malaysia using global positioning system (GPS). *ACRS 2015 - 36th Asian Conference on Remote Sensing: Fostering Resilient Growth in Asia.*
[18] Hofmann-Wellenhof, B., Lichtenegger, H., & Collins, J. (2001). Global Positioning System: Theory and Practice (5th ed.). Springer.
[19] Karaim, M. (2018, April 6). GNSS Error Sources. IntechOpen. https://www.intechopen.com/chapters/60049
[20] Dach, R., S. Lutz, P. Walser, P. Fridez (Eds); 2015: Bernese GNSS Software Version 5.2. User manual, Astronomical Institute, University of Bern, Bern Open Publishing. https://doi.org/10.7892/boris.72297; ISBN: 978-3-906813-05-9
[21] Salihin, S., Musa, T. A., & Mohd Radzi, Z. (2017). Spatio-Temporal Estimation Of Integrated Water Vapour Over The Malaysian Peninsula During Monsoon Season. *The International Archives of the Photogrammetry, Remote Sensing and Spatial Information Sciences*, XLII-4/W5, 165–175. https://doi.org/10.5194/isprs-archives-xlii 4-w5-165-2017
[22] Rothacher, M., Springer, T. A., Schaer, S., & Beutler, G. (1998). Processing Strategies for Regional GPS Networks. *Advances in Positioning and Reference Frames*, 93–100. https://doi.org/10.1007/978-3-662-03714-0_14
[23] Astudillo, J. M., Lau, L., Tang, Y. T., & Moore, T. (2018). Analysing the Zenith Tropospheric Delay Estimates in On-line Precise Point Positioning (PPP) Services and PPP Software Packages. *Sensors*, *18*(2), 580. https://doi.org/10.3390/s18020580
[24] Hlavacova, I. (2008). *Interferometric stacks in partially coherent areas* (PhD Thesis). Faculty of Civil Engineering, Czech Technical University, Prague.